Accepted Manuscript

EnKF coupled with groundwater flow moment equations applied to Lauswiesen aquifer, Germany

M. Panzeri, M. Riva, A. Guadagnini, S.P. Neuman
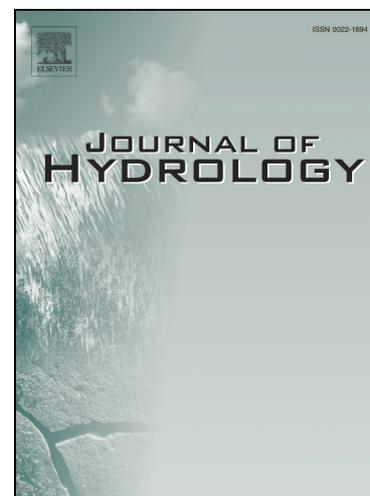
Please cite this article as: Panzeri, M., Riva, M., Guadagnini, A., Neuman, S.P., EnKF coupled with groundwater flow moment equations applied to Lauswiesen aquifer, Germany, *Journal of Hydrology* (2014), doi: http://dx.doi.org/10.1016/j.jhydrol.2014.11.057

EnKF coupled with groundwater flow moment equations applied to

Lauswiesen aquifer, Germany

M. Panzeri[1], M. Riva[1,2], A. Guadagnini[1,2], and S.P. Neuman[2]

[1]Dipartimento di Ingegneria Civile e Ambientale, Politecnico di Milano, Piazza L. Da Vinci

32, 20133 Milano, Italy

[2]Department of Hydrology and Water Resources,

University of Arizona, Tucson, Arizona 85721, USA

Details of the corresponding author:
Marco Panzeri
Ph.D.
Department of Civil and Environmental Engineering
Politecnico di Milano, Milan (Italy)
Phone: 0039 02 2399 6256
Fax: 0039 02 2399 6298
Email: marco.panzeri@polimi.it

Abstract

We describe a field application of a new data assimilation method recently proposed by Panzeri et al. (2013, 2014). The method couples a modified Ensemble Kalman Filter (EnKF) algorithm with stochastic moment equations (MEs) governing space-time variations of (theoretical ensemble) mean and covariance values of groundwater flow state variables (hydraulic heads and fluxes). Whereas traditional EnKF entails Monte Carlo (MC) simulations and suffers from inbreeding, our approach obviates both. Synthetic case studies have shown the ME-based approach to be computationally efficient and accurate when compared to MC-based results. Here we use our ME-based method to assimilate drawdown data recorded during cross-hole pumping tests in the heterogeneous alluvial Lauswiesen aquifer near Tübingen, Germany. Our results include an estimate of log transmissivity distribution throughout the aquifer and corresponding measures of estimation error. We validate our calibrated model by using it to predict drawdowns recorded during another pumping test at the site and compare its performance with that of standard MC-based EnKF.

1. Introduction

To render groundwater flow models reliable one must base them firmly on data. Regardless of whether or not these models are linear in hydraulic heads, the latter always depend in a nonlinear fashion on hydraulic conductivities or transmissivities. One way to condition models on data is via batch inverse approaches such as those examined by Zimmerman et al. (1998) or reviewed more recently by Hendricks-Franssen et al. (2009) and Zhou et al. (2014). The rapid expansion in recent decades of monitoring networks delivering high-resolution head measurements in real time through remote connections has generated widespread interest in assimilation methods capable of updating models on the basis of real-time data sequentially rather than in batch mode. Sequential data assimilation tends to be computationally more efficient than traditional batch inverse approaches. Most if not all sequential data assimilation techniques are developments on a linear filter first proposed by Kalman (1960). The purpose of this original Kalman Filter (KF) was to estimate states of linear dynamical systems on the basis of noisy temporal measurements. KF entails recursive computations of (*a*) a forecast step, in which the mean and the covariance matrix of a system state vector are propagated in time until new measurements become available, and (*b*) an analysis step, in which system states (and more recently model parameters) are updated on the basis of new data. Gelb (1994) proposed an Extended Kalman Filter (EKF) to account for model nonlinearities. EKF does so by linearizing model dynamics in each forecast step. This renders EKF (e.g., Eigbe et al., 1998; Aanonsen et al., 2009; Liu et al., 2012; Zhou et al., 2014) (a) inaccurate in cases of highly non-linear models and highly variable parameters due to rapid increase in covariance linearization error with time; and (b) computationally demanding when applied to realistically large and complex models associated with large sensitivity and error covariance matrices.

One way to assimilate data sequentially into nonlinear models is through the use of Ensemble Kalman Filters (EnKF) introduced by Evensen (1994) and modified by Burgers et al. (1998). Traditional EnKF entails generating a random sample of system state realizations through Monte Carlo (MC) solution of nonlinear dynamics equations during each forecast step, and subsequent updating of system states (and, optionally, parameters) on the basis of their MC sample mean and covariance matrix. The approach is conceptually simple and relatively easy to implement, rendering it popular among climate and other environmental modelers. Of direct relevance to this paper are synthetic EnKF studies related to subsurface flow and transport. One of these is the work of Chen and Zhang (2006) who studied the impact of MC sample size, type of measurements and timing of data assimilation on the quality of estimated model parameters; another is that of Hendricks-Franssen and Kinzelbach (2008) who explored the effects of uncertain recharge rate and transmissivity on EnKF performance. The latter authors proposed empirical strategies to circumvent, or minimize, filter inbreeding which causes EnKF to increasingly underestimate parameter estimation variance as data assimilation progresses in time. Liu et al. (2012) and Zhou et al. (2014) published detailed reviews of data assimilation and inverse modeling techniques in hydrogeology with special emphasis on EnKF. In the context of subsurface hydrology, Liu et al. (2008) used EnKF to estimate the spatial distribution of hydraulic conductivities and transport model parameters (i.e., longitudinal dispersivity and the parameters of a dual-domain mass transfer model) on the basis of hydraulic head and tracer concentration data collected at the MADE site in one year. EnKF hydraulic conductivity estimates were found to be consistent with kriged values based on flow meter measurements, which were not considered during data assimilation. Hendricks-Franssen et al. (2011) used EnKF to model variably saturated subsurface flow with river-aquifer interaction in the Limmat Valley aquifer near Zurich, Switzerland, from January 2004 till December 2007. They then used the

calibrated model to predict system dynamics from May 2009 till September 2010. Here too the ability of the model to predict hydraulic heads improved as assimilation progressed. The authors also found that overly frequent parameter updates caused model predictive capability to deteriorate due to filter inbreeding and numerical instability. Kurtz et al. (2014) used EnKF to investigate the impact of assimilating hydraulic and thermal data jointly on the estimation of system states and parameters of the Limmat Valley aquifer. They were able to assimilate a large amount of groundwater level and temperature data from the year 2007 and verify their model against numerous such data from 2011.

A review of EnKF in the context of petroleum reservoir engineering was published by Aanonsen et al. (2009). Haugen et al. (2006) used EnKF to update permeability and porosity values of a North Sea reservoir model based on a five year production record. Sequential estimates of parameters were compared with batch estimates over the entire five-year period, showing that the former reproduces observed state variables better and better as time progresses, improving upon earlier hand calibration. Bianco et al. (2007) used EnKF to estimate spatially varying model permeabilities and porosities based on three years of production data at the Zagor oil field off the West African shore. Sequential estimates of parameters based on 50, 100 and 135 MC realizations were compared with values available prior to data assimilation, once again reproducing observed state variables increasingly better as time progressed. Predictions of reservoir behavior over a subsequent 23-year time horizon, obtained with parameter estimates based on 50 Monte Carlo realizations, were better than those obtained upon relying on information available prior to data assimilation. Other examples of EnKF data assimilation in reservoir models, coupled with parameter estimation, are found in Zhang and Oliver (2011) and Emerick and Reynolds (2011).

In our view the term *ensemble* is a misnomer in the context of MC-based EnKF. We say so because in statistical mechanics and mathematical physics an ensemble, or statistical

ensemble, is typically defined as a very large (theoretically infinite) number of copies of a system. Each of these copies represents a system state so that the ensemble coincides effectively with the probability distribution for the system state under consideration (e.g., Gibbs, 1902). A new assimilation method we developed recently (Panzeri et al., 2013) is in our view validly termed EnKF precisely for this reason. Our method differs from MC-based EnKF in that it replaces MC sampling with direct computation of statistical ensemble moments. It does so by solving, in an approximate manner, exact (nonlocal, integrodifferential) equations that govern the space-time evolution of ensemble means and covariances of hydraulic heads and fluxes (Guadagnini and Neuman, 1999; Ye et al., 2004). Coupling such (ensemble) moment equations (MEs) with EnKF obviates the need for computationally intensive batch geostatistical inverse analyses of the kind described, in the context of ME, by Riva et al. (2009). In our synthetic studies (Panzeri et al., 2014) ME-based EnKF proved to be free of inbreeding issues, accurate and computationally efficient. In this paper we use our new ME-based approach to assimilate drawdown data recorded during cross-hole pumping tests in the heterogeneous alluvial Lauswiesen aquifer near Tübingen, Germany. Our results include an estimate of log transmissivity distribution throughout the aquifer and corresponding measures of estimation error. We compare our results with those obtained using standard EnKF based on various numbers of Monte Carlo realizations and validate our calibrated model against drawdowns recorded during another pumping test at the site.

2. Experimental site and available data

The Lauswiesen experimental site is located in the Neckar river valley near Tübingen, Germany. System characterization is based on information recorded at a set of monitoring and pumping wells. Local investigations reveal a relatively regular upper clay, having a thickness of 1 - 2 m, overlying conductive Quaternary sand and gravel deposits which in turn

rest on a layer of Keuper marl. The latter is usually taken to define an impervious bedrock boundary of the Quaternary sand and gravel aquifer. The aquifer has a saturated thickness of about 5 m and is characterized by a relatively stable free surface which is mainly controlled by the Neckar river water level. All boreholes penetrate the aquifer down to bedrock. Details of site hydrogeology are given by Riva et al. (2006) and references therein.

Our study focuses on the north-eastern part of this site, which covers an area of approximately 25×25 m^2. We consider transient drawdown data collected during three out of five cross-hole pumping tests conducted in fully penetrating wells B1 - B5. These and the site are depicted in Figure 1. Each test entailed pumping one of the five wells at a constant rate and observing drawdowns in the remaining four wells. Water levels, measured with transducers and recorded with data loggers (Martac and Ptak, 2003; Riva et al., 2006 and references therein), were allowed to recover fully before the start of each test. Following Neuman et al. (2007), we treat flow during each test as being horizontal and account for variation of saturated thickness by correcting the drawdown, *s*, according to (Jacob, 1944)

$$s_c = s - \frac{s^2}{2b} \tag{1}$$

where s_c is corrected drawdown and *b* is average initial saturated thickness.

Pumping test results reveal reciprocity gaps (see Bruggeman,1972; Delay et al., 2011 and references therein) between normalized drawdown curves observed when pumping from well B5 but not the other wells. Delay et al. (2011, 2012) suggest that reciprocity gaps between vertically-averaged heads monitored during two consecutive tests can be caused by various factors including (a) non-linear dependencies of local hydraulic parameters, (b) occurrence of internal boundaries within the domain, (c) inertial effects that develop through open conduits within the host rock matrix, (d) changes in aquifer properties between subsequent pumping tests, (e) contribution of the matrix pressure in monitored wells when

the behavior of the aquifer is conceptualized as a dual-continuum, (f) vertical trends in aquifer properties, and/or (g) drainage from the unsaturated zone during pumping. According to these authors, identifying the precise reasons for lack of reciprocity at a given site remains an open challenge. As drawdowns created when pumping well B5 are not reciprocal with those measured in B5 during other tests, we exclude drawdowns created by pumping well B5 from consideration in this paper. We do the same with drawdowns created by B1 some of which appear to be in error (Riva et al., 2006; Neuman et al., 2007). Our analysis is thus limited to data created by pumping in B2, B3 and B4 while monitoring all remaining wells. Corrected drawdowns corresponding to cross-hole tests in these three wells are plotted versus time on semi-logarithmic scale in Figure 2. Pumping rate, pumping duration and initial saturated thickness associated with each test are listed in Table 1. Vertical dashed lines in Figure 2 denote points in time at which data assimilation took place. Note that we limit our consideration to transient drawdowns during periods delimited by these lines, including pseudo-steady state regimes. This is to ensure that boundary effects have negligible impact on drawdowns assimilated into our model. Aquifer storativity inferred by Martac and Ptak (2003) from drawdowns recorded in pumping tests across the area range from 0.02 to 0.22, with average 0.05, all but one estimate being of order $O(10^{-2})$ m. This mild spatial variability is the reason why we, like others (e.g., Dagan, 1982; Hendricks-Franssen et al., 2011), feel justified disregarding fluctuations in storativity in comparison to those of transmissivity and considering in our analyses below aquifer storativity as a deterministic constant which we set equal to the estimated average of 0.05.

Previously Neuman et al. (2007) used type curves of Neuman et al. (2004) to estimate geometric mean transmissivity (T_G) as well as the sill (σ_Y^2) and integral scale (I_Y) of log transmissivity variogram at the site on the basis of late-time drawdown measurements. The first and last of their estimates $T_G = 2.18 \times 10^{-2}$ m^2 / s, $I_Y = 2.5$ m and $\sigma_Y^2 = 1.5$ agreed

closely with estimates $T_G = 2.38 \times 10^{-2}$ m^2/s and $\sigma_Y^2 = 1.4$ obtained independently through vertical averaging of 312 flow meter test results from 12 boreholes comprising all B wells in Figure 1c and additional seven wells shown in Figure 1b. These values are consistent with geostatistical log hydraulic conductivity estimates obtained by Lessoff et al. (2010) on the basis of aquifer direct-push slug tests (DPST) and direct-push injection logs (DPIL) across the site.

3. Numerical flow model

Our groundwater flow model uses finite elements to solve second-order (in conditional standard deviation of natural log transmissivity) approximations of otherwise exact conditional stochastic moment equations (e.g., Tartakovsky and Neuman, 1998; Ye et al., 2004; Panzeri et al., 2013). The latter nonlocal (integrodifferential) equations govern the space-time evolution of conditional ensemble means (statistical expectations) and covariances of hydraulic heads and fluxes. Our two-dimensional finite element grid, depicted in Figure 3, contains 79 × 79 rectangular elements that decrease in size toward the center of the 356.2 × 356.2 m^2 study area. The finer inner part of the grid, including wells B1 - B5, contains 39 × 39 square elements of size 0.6 × 0.6 m^2. Log transmissivities within this inner area are uniform in each element and treated as an autocorrelated random field, *Y*. Rectangular elements in the outer area are assigned a single deterministic transmissivity equal to the geometric mean, $T_G = 2.18 \times 10^{-2}$ m^2/s, estimated for this site by Neuman et al. (2007). As noted earlier, we limit our analysis to drawdowns in the fine inner region of the grid, occurring prior to the onset of boundary effects in this region. Similar to Riva et al. (2009), we performed tests about the suitability of the grid size upon comparing numerical results against the Theis model (Theis, 1935) in a homogeneous setting. Comparison between analytical and numerical solutions shows negligible differences for the grid size we employ. This is documented in Figure 4, which depicts the temporal evolution of the absolute

difference, E_h, between analytical and numerical heads evaluated at the locations of the observation wells for the tests we analyze. These plots demonstrate that numerical errors associated with grid discretization are always well below 10^{-3} m, this being the value we employed for standard deviation of head measurement errors.

Initial heads across the domain are zero, as is head on all four domain boundaries. Pumping in each test is represented by a point sink, $Q_P \delta(\mathbf{x} - \mathbf{x_w})$, in which Q_P is withdrawal rate, δ is the Dirac delta function and $\mathbf{x_w}$ is position vector of the pumping well, all wells being located at grid nodes. Disregarding pumping well radius and storage in this manner is likely to introduce inaccuracies in the reproduction of pumping well drawdowns, which we therefore do not assimilate.

4. Data assimilation strategy

We employ our ME-based EnKF algorithm to assimilate drawdowns recorded during tests T2 and T3 at points in time indicated by vertical dashed lines in Figure 2. The mean and covariance of Y estimated on the basis of T2 are used to initiate the assimilation of T3 data. Results are validated against drawdowns recorded during test T4.

Drawdowns in Figure 2 are recorded at more than 100 time steps during each test of duration close to 10,000 s. Previous studies (e.g., Chen and Zhang, 2006; Panzeri et al., 2013) have shown that (*a*) hydraulic heads measured during the early transient regime are associated with higher information content than those registered during the later pseudo-steady state regime and (*b*) switching from low to high temporal assimilation frequency yields only marginal improvement in parameter estimates. For these reasons, and to lower computational cost, we assimilate drawdowns only at 15 points in time during each test such that about 80% of the assimilated data correspond to early transient flow.

As detailed by Ye et al. (2004), we solve our MEs at a fixed number of discretization points in Laplace space and back-transform their solution into the time domain using a

quotient-difference algorithm developed by De Hoog et al. (1982). The computational time required for any forward solution step is thus constant, independent of temporal time step size. This allows us to restart the flow simulation from time zero after each update, thereby conserving mass prior to any such update. Additionally, since the Kalman gain matrix requires only cross-covariances between heads at observation well nodes and log transmissivities at grid elements, our approach avoids the need to compute entire head covariance matrices. It thus results in significant speed-up of the ME-based assimilation algorithm.

5. Theoretical background and data assimilation algorithm

We define the state vector

$$\mathbf{y} = \begin{bmatrix} \mathbf{Y} \\ \mathbf{s} \end{bmatrix} \tag{2}$$

where $\mathbf{Y}$ and $\mathbf{s}$ are vectors containing log transmissivities at the N_Y grid elements and drawdowns at the N_s grid nodes, respectively, so that $\mathbf{y}$ has dimension $N_y = N_Y + N_s$. We denote by $T_0 = 0$ the starting time of each pumping test and by T_k ($k = 1, 2, ..., 15$) the points in time at which drawdown measurements are assimilated during each pumping test. Due to incomplete knowledge of transmissivity the vector $\mathbf{y}$ is modeled as a random field. We link head observations to unknown values of $\mathbf{y}$ at time T_k, $\mathbf{y}^{T_k}$, through

$$\mathbf{d}^{T_k} = \mathbf{H}^{T_k}\mathbf{y}^{T_k} + \boldsymbol{\varepsilon}^{T_k} \tag{3}$$

where the vector $\mathbf{d}^{T_k}$ contains N_d measurements at time T_k which, in our case, consist of $N_d = 4$ heads at observation wells; $\mathbf{H}^{T_k}$ is a transformation matrix of size $N_d \times N_y$; and $\boldsymbol{\varepsilon}^{T_k}$ is a random vector representing zero-mean Gaussian measurement errors with covariance matrix $\boldsymbol{\Sigma}_{\boldsymbol{\varepsilon}\boldsymbol{\varepsilon}}$. In our application, entries $H_{ij}^{T_k}$ of $\mathbf{H}^{T_k}$ are equal to 1 when element j of vector $\mathbf{y}^{T_k}$ corresponds to observed drawdown constituting entry i of $\mathbf{d}^{T_k}$ and 0 otherwise. We further

assume that measurement errors are mutually uncorrelated with standard deviation $\sigma_\varepsilon = 0.001$ m (rendering $\boldsymbol{\Sigma}_{\varepsilon\varepsilon}$ diagonal and homoscedastic), independent of measurement location. As assimilated drawdowns, s_c, range between 0.01 m and 0.10 m, the ratios σ_ε / s_c range from 10^{-1} to 10^{-2}. We collect all measurement vectors up to time T_k (i.e., $\mathbf{d}^{T_i}$, $i = 1, \ldots k$) in a matrix $\mathbf{D}^{T_k}$ and denote the state vector $\mathbf{y}$ at time T_k, conditioned on $\mathbf{D}^{T_{k-1}}$ and $\mathbf{D}^{T_k}$ respectively, by $\mathbf{y}^{f,T_k}$ and $\mathbf{y}^{u,T_k}$.

Our data assimilation strategy, based on the methodology of Panzeri et al. (2013), requires assigning initial mean and covariance values to $\mathbf{y}^{u,T_0}$ during each pumping test. To initiate the assimilation of test T2 data we condition the first two statistical moments of $\mathbf{Y}$ on those provided by type curve analysis of Neuman et al. (2007). Correspondingly, all elements of the mean vector $\left\langle \mathbf{Y}^{u,T_0} \right\rangle$ are set equal to the mean log transmissivity estimate, $\ln\left(2.18 \times 10^{-2}\right) = -3.826$ (where transmissivity is measured in m^2/s), while those of the corresponding covariance matrix, $\mathbf{C}_{\mathbf{Y}}^{u,T_0}$, are evaluated on the basis of an exponential isotropic variogram with sill $\sigma_Y^2 = 1.5$ and integral scale $I_Y = 2.5$ m. To initiate the assimilation of test T3 data we adopt mean and covariance values from the end of T2 assimilation. We set initial drawdowns at time T_0 equal to steady-state mean drawdowns in the absence of pumping. In our case this yields zero values for all elements of the initial mean drawdown vector, $\left\langle \mathbf{s}^{u,T_0} \right\rangle$, covariance matrix, $\mathbf{C}_{\mathbf{s}}^{u,T_0}$, and cross-covariance matrix between drawdowns and log transmissivities, $\mathbf{C}_{\mathbf{sY}}^{u,T_0}$.

At assimilation steps $T_{k>0}$ we evaluate the first two moments of $\mathbf{y}^{f,T_k}$, i.e., $\left\langle \mathbf{y}^{f,T_k} \right\rangle$ and $\boldsymbol{\Sigma}_{\mathbf{yy}}^{f,T_k}$, by solving the stochastic MEs of transient groundwater flow for the time interval $\left(T_0 \quad T_k\right]$ subject to zero initial drawdown while setting the mean and covariance of $\mathbf{Y}$ equal

to their estimates, $\left\langle \mathbf{Y}^{u,T_{k-1}} \right\rangle$ and $\mathbf{C}_{\mathbf{Y}}^{u,T_{k-1}}$, at assimilation step T_{k-1}. Moments of the updated

vector $\mathbf{y}^{u,T_k}$ are then computed with the aid of $\mathbf{d}^{T_k}$, representing measurements at time T_k,

according to

$$\left\langle \mathbf{y}^{u,T_k} \right\rangle = \left\langle \mathbf{y}^{f,T_k} \right\rangle + \mathbf{K}^{T_k} \left[\mathbf{d}^{T_k} - \mathbf{H}^{T_k} \left\langle \mathbf{y}^{f,T_k} \right\rangle \right] = \begin{bmatrix} \left\langle \mathbf{Y}^{u,T_k} \right\rangle \\ \left\langle \mathbf{s}^{u,T_k} \right\rangle \end{bmatrix} \tag{4}$$

$$\boldsymbol{\Sigma}_{\mathbf{yy}}^{u,T_k} = \left(\mathbf{I}_{N_y} - \mathbf{K}^{T_k} \mathbf{H}^{T_k} \right) \boldsymbol{\Sigma}_{\mathbf{yy}}^{f,T_k} = \begin{bmatrix} \mathbf{C}_{\mathbf{Y}}^{u,T_k} & \mathbf{C}_{\mathbf{Ys}}^{u,T_k} \\ \mathbf{C}_{\mathbf{sY}}^{u,T_k} & \mathbf{C}_{\mathbf{s}}^{u,T_k} \end{bmatrix} \tag{5}$$

in which

$$\mathbf{K}^{T_k} = \boldsymbol{\Sigma}_{\mathbf{yy}}^{f,T_k} \left(\mathbf{H}^{T_k} \right)^{+} \left[\boldsymbol{\Sigma}_{\boldsymbol{\varepsilon\varepsilon}}^{T_k} - \mathbf{H}^{T_k} \boldsymbol{\Sigma}_{\mathbf{yy}}^{f,T_k} \left(\mathbf{H}^{T_k} \right)^{+} \right]^{-1} \tag{6}$$

is the Kalman gain matrix, the superscript + denoting transpose.

6. Results and discussion

Figures 5 and 6 depict spatial distributions of estimated log transmissivity mean and

variance at selected assimilation time steps during tests T2 and T2+T3, respectively. The

mean Y field in Figure 5 starts displaying significant heterogeneity after the first assimilation

step. As expected, results vary faster during early updating steps than during later steps.

Estimation variance is smallest near wells B1, B2 and B3 and larger near wells B4 and B5

that are located farthest from pumping well B2. As expected, the variance increases toward

its unconditional value (equal to the variogram sill) with distance from these wells. The

assimilation of additional data in Figure 6 is seen to yield only minor changes to the mean

and variance of Y in Figure 5. Though based on diverse data and methods, these results as

well as those shown in Figures A.1 and A.2 (Appendix A) are consistent with a relatively low

variance obtained by Lessoff et al. (2010) for hydraulic conductivities close to well B2.

Figure 7 depicts the temporal behavior of spatially averaged Y estimation variance, V_Y,

$$V_Y = \frac{1}{N_Y^*} \sum_{i=1}^{N_Y} \sigma_Y^{2\,u,t^*}(\mathbf{x}_i) \qquad (7)$$

in which $\sigma_Y^{2\,u,t^*}(\mathbf{x}_i)$ is log transmissivity estimation variance in grid element i, N_Y^* is number of elements in the dense inner portion of the grid (Figure 3), and $t^* = t/T_{N_k}$ is normalized time. As already noted, V_Y decreases fastest during early steps of test T2 assimilation, more slowly during early steps of T3 assimilation, and slower yet at later steps of each assimilation sequence. Total decrease in V_Y is 14 % during the first assimilation and 5 % during the second.

Figures 8 - 11 compare drawdowns recorded in wells B1, B2, B3 and B5, respectively, while pumping well B4 during test T4 with corresponding estimates of mean drawdown and ± 2 standard deviations about the mean while relying on prior Y values, estimates based on assimilation of T2 data, and estimates based on joint assimilation of T2 and T3 data. Figures 8 – 10 confirm that (a) relying on prior parameter estimates results in poor drawdown fits and wide uncertainty ranges, (b) assimilating T2 data improves fits and reduces uncertainty significantly, while (c) further assimilation of T3 data bring about only marginal improvements in fit and uncertainty reduction. Poor fits in Figure 11 confirm that drawdowns in well B5 are not represented accurately by our model. As discussed by Delay et al. (2011, 2012), these can be ascribed to the inability of typical mathematical formulations of fully saturated groundwater flow to reproduce reciprocity gaps. This element does not invalidate the quality of our calibration. Figure 12 indicates percent χ of drawdown data recorded in B1, B2, and B3 during test T4 that fall inside the corresponding uncertainty bounds in Figures 8 – 10. On average, χ increases from 12% prior to assimilation to about 40% after joint assimilation of T2 and T3 data.

Next we examine the effect of adding T4 drawdown data to our assimilation sequence using the same approach as earlier. Figure 13 depicts spatial distributions of estimated log transmissivity mean and variance at selected assimilation time steps during this test. Results differ slightly from those following joint assimilation of T2 and T3 data in Figure 6 by an increase in mean Y values at the top-right of the grid and a slight decrease in variance throughout the domain.

Finally we compare our estimates based on T2 data to those obtained for this case using traditional MC-based EnKF. Implementation and results of this analysis are described in Appendix A. Results of MC-based EnKF approach those of ME-based EnKF as the number of realizations increases from 5,000 to 50,000. With such a large number of realizations MC-based EnKF becomes computationally more demanding than our ME-based approach.

7. Conclusions

Our work leads to the following major conclusions.

1. The moment-equations (ME) based ensemble Kalman filter (EnKF) approach to data assimilation proposed by Panzeri et al. (2013) works well when applied to three sets of pumping test data from the Lauswiesen alluvial aquifer near Tübingen, Germany. The approach provides sequential estimates of log transmissivity and its variance-covariance distributions in space.

2. Estimates obtained through assimilation of data from two pumping tests were validated successfully against a third such test at the site. Consistent with observations by Chen and Zhang (2006) and Panzeri et al. (2013) on synthetic scenarios, our parameter estimates improved faster when based on the assimilation of transient drawdown data than when based on near-steady state data.

3. We found that to reduce parameter estimation error by as much as was possible using our ME-based EnKF approach, the traditional Monte Carlo-based approach would require so many simulations as to render it computationally less efficient.

Acknowledgements

References

Aanonsen, S.I., Nævdal, G., Oliver, D.S., Reynolds, A.C., Vallès, B., 2009. The ensemble Kalman filter in reservoir engineering – a review. SPE J. 14 (3), 393-412. http://dx.doi.org/10.2118/117274-PA.

Bianco, A., Cominelli, A., Dovera, L., Nævdal, G., Vallès, B., 2007. History matching and production forecast uncertainty by means of the ensemble Kalman filter: A real field application. In: 69th EUROPEC/EAGE Conference and Exhibition 2007, London, U.K. 2, 1046-1056. http://dx.doi.org/10.2118/107161-MS.

Bruggeman, G.A., 1972. The reciprocity principle in flow through heterogeneous porous media. In: Fundamentals of transport in porous media. Amsterdam: IAHR Publications, Elsevier, 135-149.

Burgers, G., van Leeuwen, P.J., Evensen, G., 1998. Analysis Scheme in the Ensemble Kalman Filter. Mon. Wea. Rev. 126 (6), 1719–1724. http://dx.doi.org/10.1175/1520-0493(1998)126%3C1719:ASITEK%3E2.0.CO;2.

Chen, Y., Zhang, D., 2006. Data assimilation for transient flow in geologic formations via ensemble Kalman filter. Adv. Water Resour. 29 (8), 1107-1122. http://dx.doi.org/10.1016/j.advwatres.2005.09.007.

Dagan, G., 1982. Analysis of flow through heterogeneous random aquifers: 2. Unsteady flow in confined formations, Water Resour. Res. 18 (5), 1571-1585. http://dx.doi.org/10.1029/WR018i005p01571.

De Hoog, F.R., Knight, J.H., Stokes, A.N., 1982. An improved method for numerical inversion of Laplace transform. SIAM J. Sci. Stat. Comput. 3 (3), 357-366. http://dx.doi.org/10.1137/0903022.

Delay, F., Ackerer, P., Guadagnini, A., 2011. Theoretical analysis and field evidence of reciprocity gaps during interference pumping tests. Adv. Water Resour. 34 (5), 592-606. http://dx.doi.org/ 10.1016/j.advwatres.2011.02.006.

Delay, F., Ackerer, P., Guadagnini, A., 2012. On the emergence of reciprocity gaps during interference pumping tests in unconfined aquifers, Adv. Water Resour. 46, 11-19. http://dx.doi.org/10.1016/j.advwatres.2012.06.002.

Deutsch, C.V., Journel, A.G., 1997. GSLIB, geostatistical software library and user's guide. second ed. Oxford University Press, New York.

Eigbe, U., Beck, M.B., Wheater, H.S., Hirano, F., 1998. Kalman filtering in groundwater flow modelling: problems and prospects, Stochastic Hydrology and Hydraulics, 12 (1), 15-32. http://dx.doi.org/10.1007/s004770050007.

Emerick, A.A., Reynolds, A.C., 2011. History Matching a Field Case Using the Ensemble Kalman Filter With Covariance Localization, SPE Reserv. Eval. Eng. 14 (4), 423-432. http://dx.doi.org/10.2118/141216-PA.

Evensen, G., 1994. Sequential data assimilation with a nonlinear quasi-geostrophic model using Monte Carlo methods to forecast error statistics. J. Geophys. Res. 99(C5), 10143-10162. http://dx.doi.org/10.1029/94JC00572.

Gelb, A., 1994. Applied optimal estimation. The MIT Press.

Gibbs, J.W., 1902. Elementary Principles in Statistical mechanics, Dover Publications Inc., New York.

Guadagnini, A., Neuman, S.P., 1999. Nonlocal and localized analyses of conditional mean steady state flow in bounded, randomly nonuniform domains: 1. Theory and computational approach. Water Resour. Res. 35 (10), 2999-3018. http://dx.doi.org/10.1029/1999WR900160.

Haugen, V., Natvik, L.J., Evensen, G., Berg, A.M., Flornes, K.M., Naevdal, G., 2006. History Matching Using the Ensemble Kalman Filter on a North Sea Field Case, SPE Annual Technical Conference and Exhibition, San Antonio, Texas, USA. http://dx.doi.org/10.2118/102430-MS.

Hendricks Franssen, H.J., Kinzelbach, W., 2008. Real-time groundwater flow modeling with the Ensemble Kalman Filter: Joint estimation of states and parameters and the filter imbreeding problem. Water Resour. Res. 44 (9), W09408. http://dx.doi.org/10.1029/2007WR006505.

Hendricks Franssen, H.J., Alcolea, A., Riva, M., Bakr, M., van der Wiel, N., Stauffer, F., Guadagnini, A., 2009. A comparison of seven methods for the inverse modelling of groundwater flow. Application to the characterisation of well catchments, Adv. Water Resour. 32 (6), 851-872. http://dx.doi.org/10.1016/j.advwatres.2009.02.011.

Hendricks Franssen, H.J., Kaiser, H.P., Kuhlmann, U., Bauser, G., Stauffer, F., Muller, R., Kinzelbach, W., 2011. Operational real-time modeling with ensemble Kalman Filter of variably saturated subsurface flow including stream-aquifer interaction and parameter updating. Water Resour. Res. 47 (2), W02532. http://dx.doi.org/10.1029/2010WR009480.

Jacob, C.E., 1944. Notes on determining permeability by pumping tests under water-table conditions, mimeo report, U.S. Geol. Surv., Reston, Va, USA.

Kalman, R.E., 1960. A New Approach to Linear Filtering and Prediction Problems, J. Basic Eng., 82(D), 35-45, http://dx.doi.org/10.1115/1.3662552.

Kurtz, W., Hendricks Franssen, H.J., Kaiser, H.P., Vereecken, H., 2014. Joint assimilation of piezometric heads and groundwater temperatures for improved modeling of river-aquifer interactions. Water Resour. Res. 50 (2), 1665-1688. http://dx.doi.org/10.1002/2013WR014823.

Lessoff, S.C., Schneidewind, U., Leven, C., Blum, P., Dietrich, P., Dagan, G., 2010. Spatial characterization of the hydraulic conductivity using direct-push injection logging, Water Resour. Res., 46, W12502, http://dx.doi.org/10.1029/2009WR008949.

Liu, G., Chen, Y., Zhang, D., 2008. Investigation of flow and transport processes at the MADE site using ensemble Kalman filter. Adv. Water Resour. 31 (7), 975-986. http://dx.doi.org/10.1016/j.advwatres.2008.03.006.

Liu, H., Weerts, A.H., Clark, M., Hendricks Franssen, H.J., Kumar, S., Moradkhani, H., Seo, D.J., Schwanenberg, D., Smith, P., van Dijk, A.I.J.M., van Velzen, N., He, M., Lee, H., Noh, S.J., Rakovec, O., Restrepo, P., 2012. Advancing data assimilation in operational hydrologic forecasting: progresses, challenges, and emerging opportunities. Hydrol. Earth Syst. Sci. 16(10), 3863-3887. http://dx.doi.org/10.5194/hess-16-3863-2012.

Martac, E., Ptak, T., 2003. Data sets for transport model calibration/validation, parameter upscaling studies and testing of stochastic transport models/theory. Report D16 of Project "Stochastic Analysis of Well-Head Protection and Risk Assessment - W-SAHaRA", EU contract EVK1-CT-1999-00041, Dipartimento Ingegneria Idraulica, Ambientale, Infrastrutture Viarie, Rilevamento, Politecnico di Milano, Milan, Italy.

Neuman, S.P., Guadagnini, A., Riva, M., 2004. Type-curve estimation of statistical heterogeneity. Water Resour. Res. 40 (4), W04201. http://dx.doi.org/10.1029/2003WR002405.

Neuman, S.P., Blattstein, A., Riva, M., Tartakovsky, D.M., Guadagnini, A., Ptak, T., 2007. Type curve interpretation of late-time pumping test data in randomly heterogeneous aquifers, Water Resour. Res. 43 (10), W10421. http://dx.doi.org/10.1029/2007WR005871.

Panzeri, M., Riva, M., Guadagnini, A., Neuman, S.P., 2013. Data assimilation and parameter estimation via ensemble Kalman filter coupled with stochastic moment equations of

transient groundwater flow. Water Resour. Res. 49 (3), 1334-1344. http://dx.doi.org/10.1002/wrcr.20113.

Panzeri, M., Riva, M., Guadagnini, A., Neuman, S.P., 2014. Comparison of Ensemble Kalman Filter groundwater-data assimilation methods based on stochastic moment equations and Monte Carlo simulation. Adv. Water Resour. 66, 8-18. http://dx.doi.org/10.1016/j.advwatres.2014.01.007.

Riva, M., Guadagnini, L., Guadagnini, A., Ptak, T., Martac, E., 2006. Probabilistic study of well capture zones distribution at the Lauswiesen field site. J. Contam. Hydrol. 88 (1-2), 92-118. http://dx.doi.org/10.1016/j.jconhyd.2006.06.005.

Riva, M., Guadagnini, A., Neuman, S.P., Bianchi Janetti, E., Malama, B., 2009. Inverse analysis of stochastic moment equations for transient flow in randomly heterogeneous media. Adv. Water Resour. 32 (10), 1495-1507. http://dx.doi.org/10.1016/j.advwatres.2009.07.003.

Tartakovsky, D.M., Neuman, S.P., 1998. Transient flow in bounded randomly heterogeneous domains 1. Exact conditional moment equations and recursive approximations. Water Resour. Res. 34 (1), 1-12. http://dx.doi.org/10.1029/97WR02118.

Theis, C.V., 1935. The relation between the lowering of the piezometric surface and the rate and duration of discharge of a well using groundwater storage. Eos Trans. AGU, 16, 519.

Ye, M., Neuman, S.P., Guadagnini, A., Tartakovsky, D.M., 2004. Nonlocal and localized analyses of conditional mean transient flow in bounded, randomly heterogeneous porous media. Water Resour. Res. 40 (5), W05104. http://dx.doi.org/10.1029/2003WR002099.

Zhang, Y., Oliver, D.S., 2011. History Matching Using the Ensemble Kalman Filter With Multiscale Parameterization: A Field Case Study. SPE J. 16 (2), 307-317. http://dx.doi.org/10.2118/118879-PA.

Zimmerman, D.A., De Marsily, G., Gotway, C.A., Marietta, M.G., Axness, C.L., Beauheim, R.L., Bras, R.L., Carrera, J., Dagan, G., Davies, P.B., et al., 1998. A comparison of seven geostatistically based inverse approaches to estimate transmissivities for modeling advective transport by groundwater flow, Water Resour. Res., 34 (6), 1373-413. http://dx.doi.org/10.1029/98WR00003.

Zhou, H., Gómez-Hernández, J.J., Li, L., 2014. Inverse methods in hydrogeology: Evolution and recent trends. Adv. Water Resour. 63, 22-37. http://dx.doi.org/10.1016/j.advwatres.2013.10.014.

Appendix A - Comparison of ME- and MC-based EnKF

We compare results obtained through our ME-based EnKF assimilation of T2 drawdown data against those obtained with traditional EnKF based on MC simulation. The assimilation is initialized by generating a collection of log transmissivity realizations, $\mathbf{Y}_i^{u,T_0}$, $i = 1,\ldots, NMC$, where NMC is the size of the MC sample. This is done by means of a Sequential Gaussian Simulator SGSIM (Deutsch and Journel, 1997) employing the same variogram parameters as those used for our ME-based analysis. Forward state vectors at time steps T_k, $\mathbf{y}_i^{f,T_k}$, $i = 1,\ldots, NMC$, are obtained through deterministic flow simulations over time intervals $(T_0, \quad T_k]$ using estimates $\mathbf{Y}_i^{u,T_{k-1}}$ and uniform zero initial drawdown. As in the ME-based case, we solve the flow equations in Laplace space and back transform the results numerically into the time domain.

The collection of forward state vectors are then updated according to

$$\mathbf{y}_i^{u,T_k} = \mathbf{y}_i^{f,T_k} + \hat{\mathbf{K}}^{T_k}\left(\mathbf{d}_i^{T_k} - \mathbf{H}^{T_k}\mathbf{y}_i^{f,T_k}\right) \qquad\qquad i = 1,\ldots, NMC \qquad\qquad (A.1)$$

where $\mathbf{d}_i^{T_k}$ is obtained by perturbing the observation vector available at time step T_k, $\mathbf{d}^{T_k}$, with a realization $\boldsymbol{\varepsilon}_i^{T_k}$ of the random vector $\boldsymbol{\varepsilon}^{T_k}$

$$\mathbf{d}_i^{T_k} = \mathbf{d}^{T_k} + \boldsymbol{\varepsilon}_i^{T_k} \qquad\qquad\qquad\qquad (A.2)$$

and $\hat{\mathbf{K}}^{T_k}$ is the approximated Kalman gain matrix evaluated through

$$\hat{\mathbf{K}}^{T_k} = \hat{\boldsymbol{\Sigma}}_{\mathbf{yy}}^{f,T_k}\left(\mathbf{H}^{T_k}\right)^+\left[\hat{\boldsymbol{\Sigma}}_{\boldsymbol{\varepsilon\varepsilon}}^{T_k} - \mathbf{H}^{T_k}\hat{\boldsymbol{\Sigma}}_{\mathbf{yy}}^{f,T_k}\left(\mathbf{H}^{T_k}\right)^+\right]^{-1} \qquad\qquad (A.3)$$

in which $\hat{\boldsymbol{\Sigma}}_{\mathbf{yy}}^{f,T_k}$ and $\hat{\boldsymbol{\Sigma}}_{\boldsymbol{\varepsilon\varepsilon}}^{T_k}$ are the sample covariance matrices of the vectors $\mathbf{y}_i^{f,T_k}$ and $\boldsymbol{\varepsilon}_i^{T_k}$, $i = 1,\ldots, NMC$, respectively.

We assimilate the observations registered during test T2 adopting the same strategy described in Section 4 and investigate the effect of adopting diverse sizes of the MC sample (i.e., we employ $NMC = 500$; 5,000 and 50,000). Figures A.1 and A.2 compare spatial distributions of

corresponding log transmissivity mean and variance, respectively, at selected time steps with ME- and MC-based EnKF methodologies. Figure A.1 shows that employing $NMC = 500$ MC realizations does not yield stable mean log transmissivities, requiring at least $NMC = 5000$ realizations to identify the site heterogeneity pattern clearly. Mean and variance values obtained with a sufficiently large number of MC realizations are similar to those obtained with the ME-based approach.

Both approaches were implemented in parallel using a similar number and type (Intel i7-3930K) of processors. Whereas running one assimilation step of ME-based EnKF required approximately 3 hours, running 500, 5,000 and 50,000 MC realizations required about 1, 6 and 60 hours, respectively. We thus see that embedding MEs in EnKF yields results of similar quality to those obtained with a large number of MC realizations, which however requires more computational time. An additional disadvantage of the MC-based approach is that it requires assessing the rates at which sample statistics converge to their unknown ensemble values.
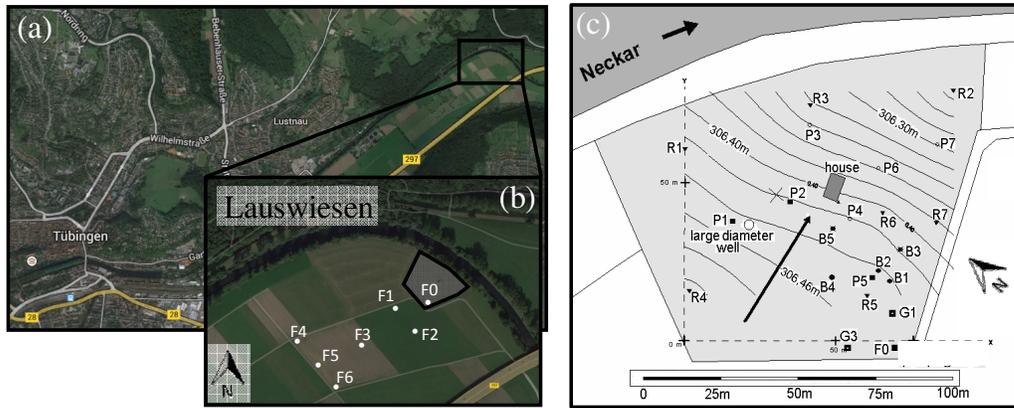
Figure 1. (a, b) Satellite images of Lauswiesen site (from Google Earth); (c) spatial location of wells, piezometric surface (isolines) and average groundwater flow direction (black arrow) in study area. Boreholes marked as R- P- and G- have been employed in prior experimental campaigns and are not part of the cross-hole pumping test sequence here analyzed.
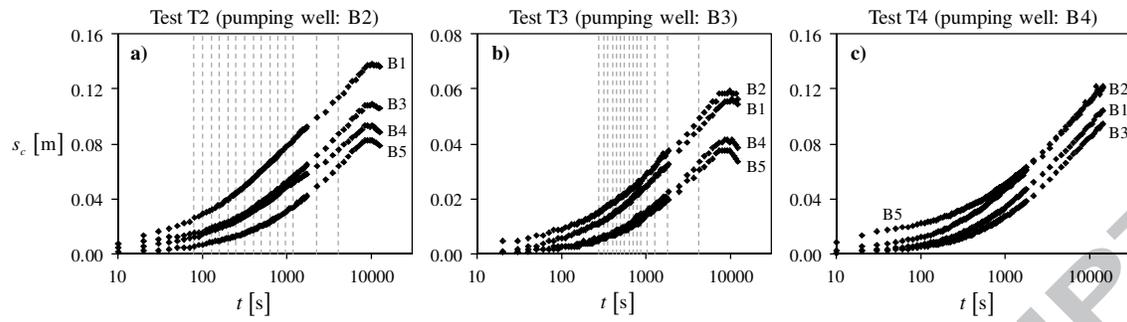
Figure 2. Corrected drawdowns recorded while pumping from wells B2, B3 or B4 versus time. Vertical dashed lines show when assimilation took place during tests T2 and T3.
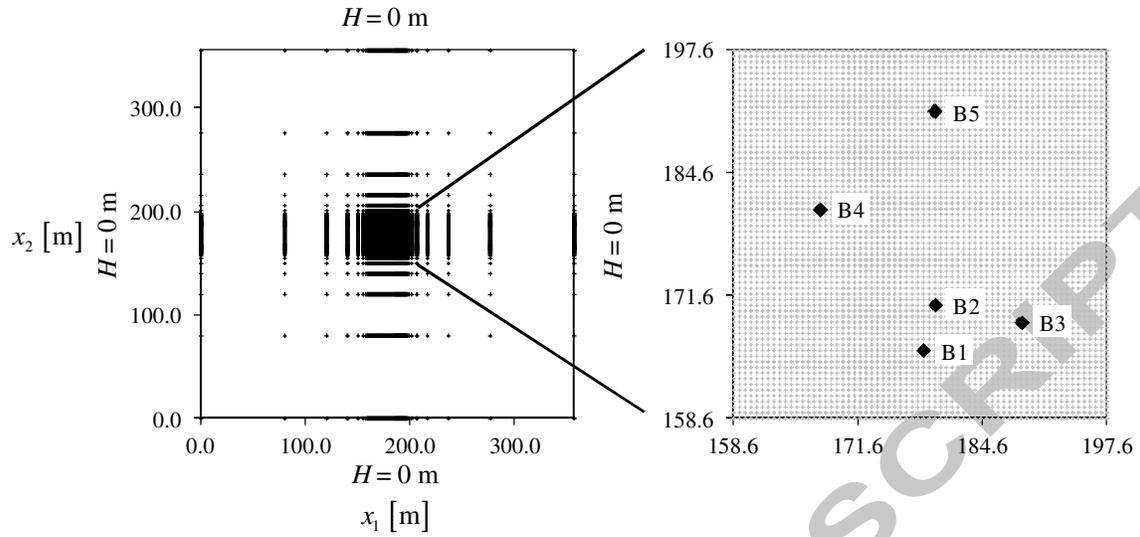
Figure 3. Flow domain, details of numerical grid (+), boundary conditions and spatial locations of wells B1 - B5.
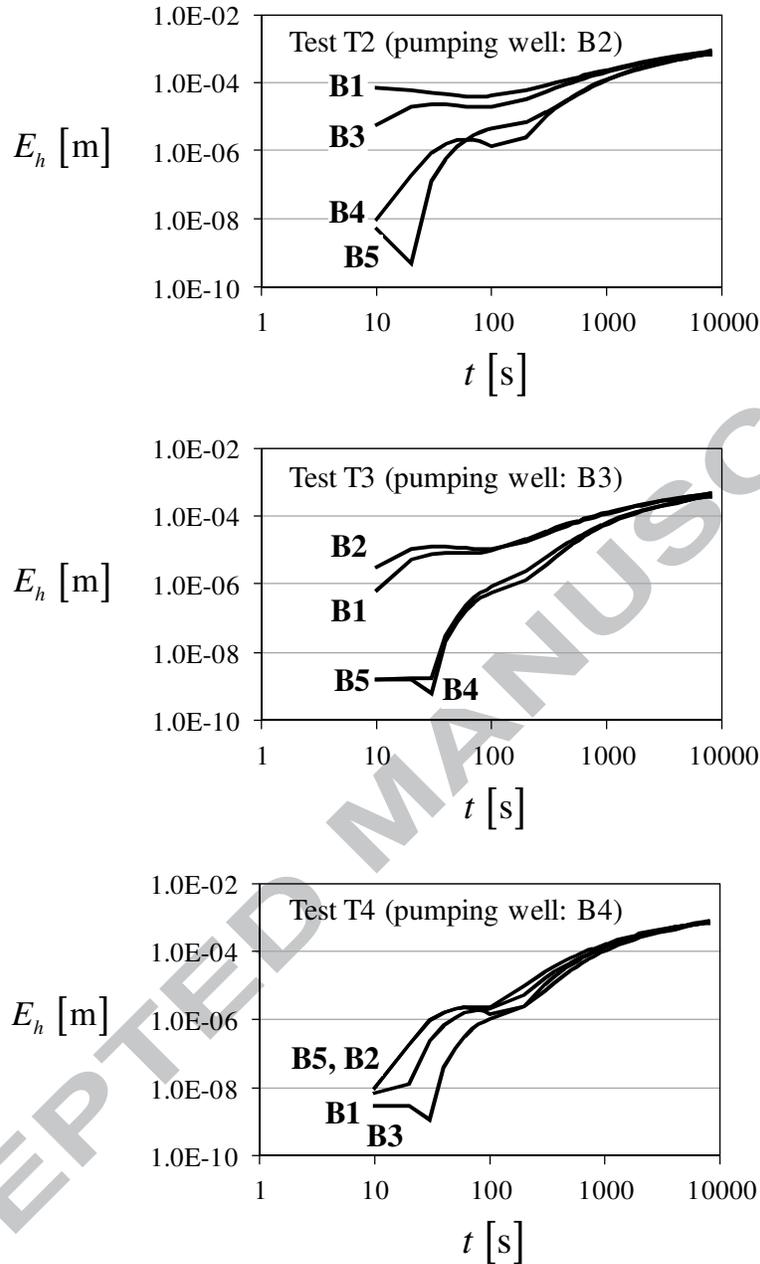
Figure 4. Comparison between numerical results and Theis model [*Theis*, 1935] in a homogeneous setting. Temporal evolution of absolute difference, E_h, between analytical and numerical heads evaluated at observation wells.

k	$\left\langle \mathbf{Y}^{u,T_k} \right\rangle$	$\sigma_Y^{2\ u,T_k}$
0		
1		
5		
10		
15		

-7   -4   -1   2   0   0.5   1   1.5
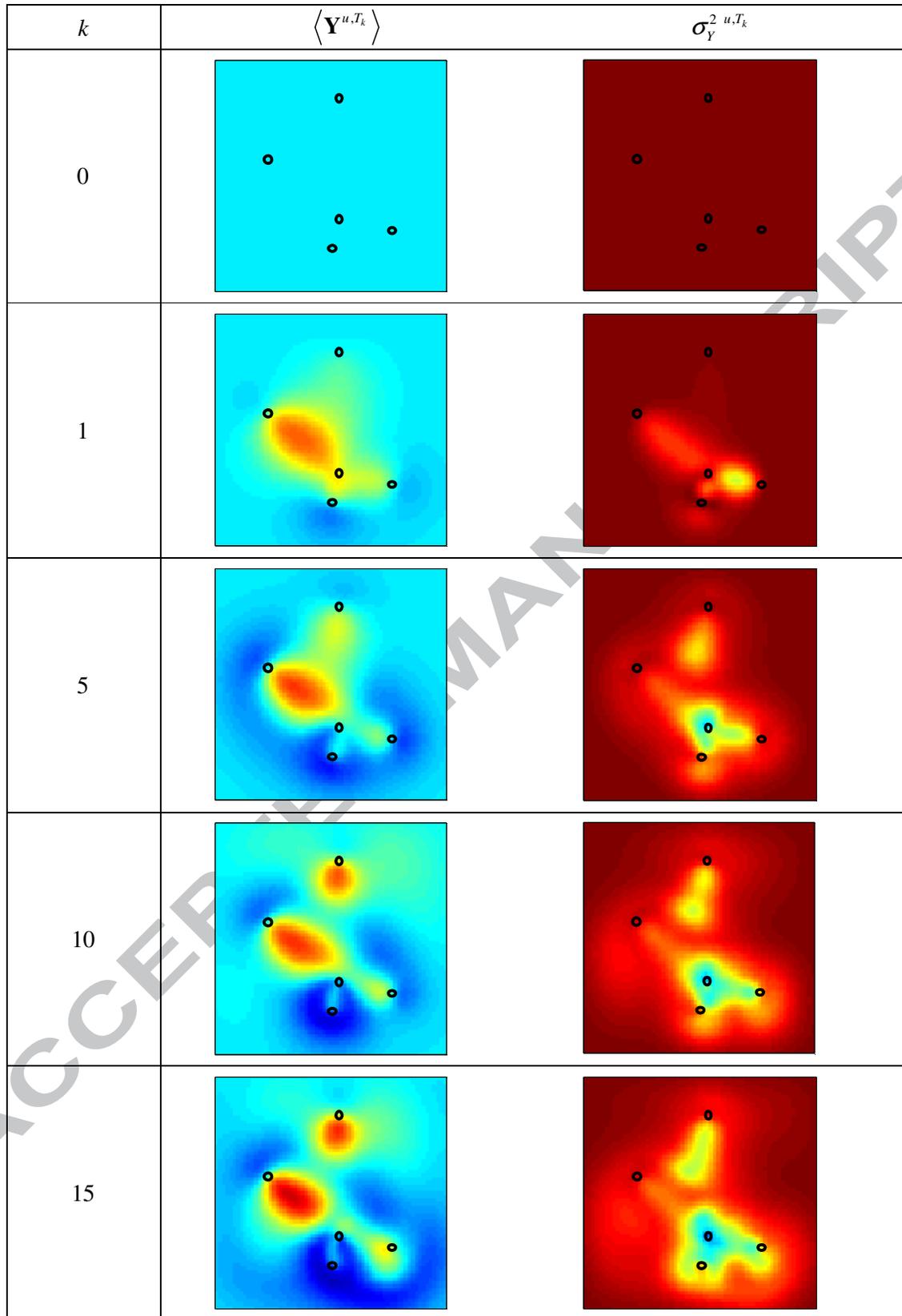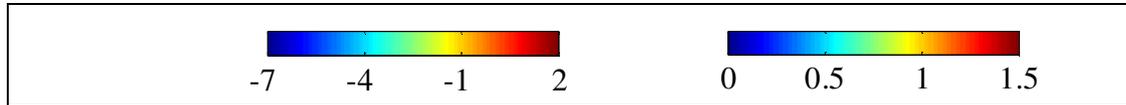
Figure 5. Spatial distributions of estimated log transmissivity mean and variance at assimilation steps k of drawdowns measured during test T2 while pumping well B2. Circles indicate spatial locations of wells B1 - B5.

k	$\left\langle \mathbf{Y}^{u,T_k} \right\rangle$	$\sigma_Y^{2\ u,T_k}$
0		
1		
5		
10		
15		
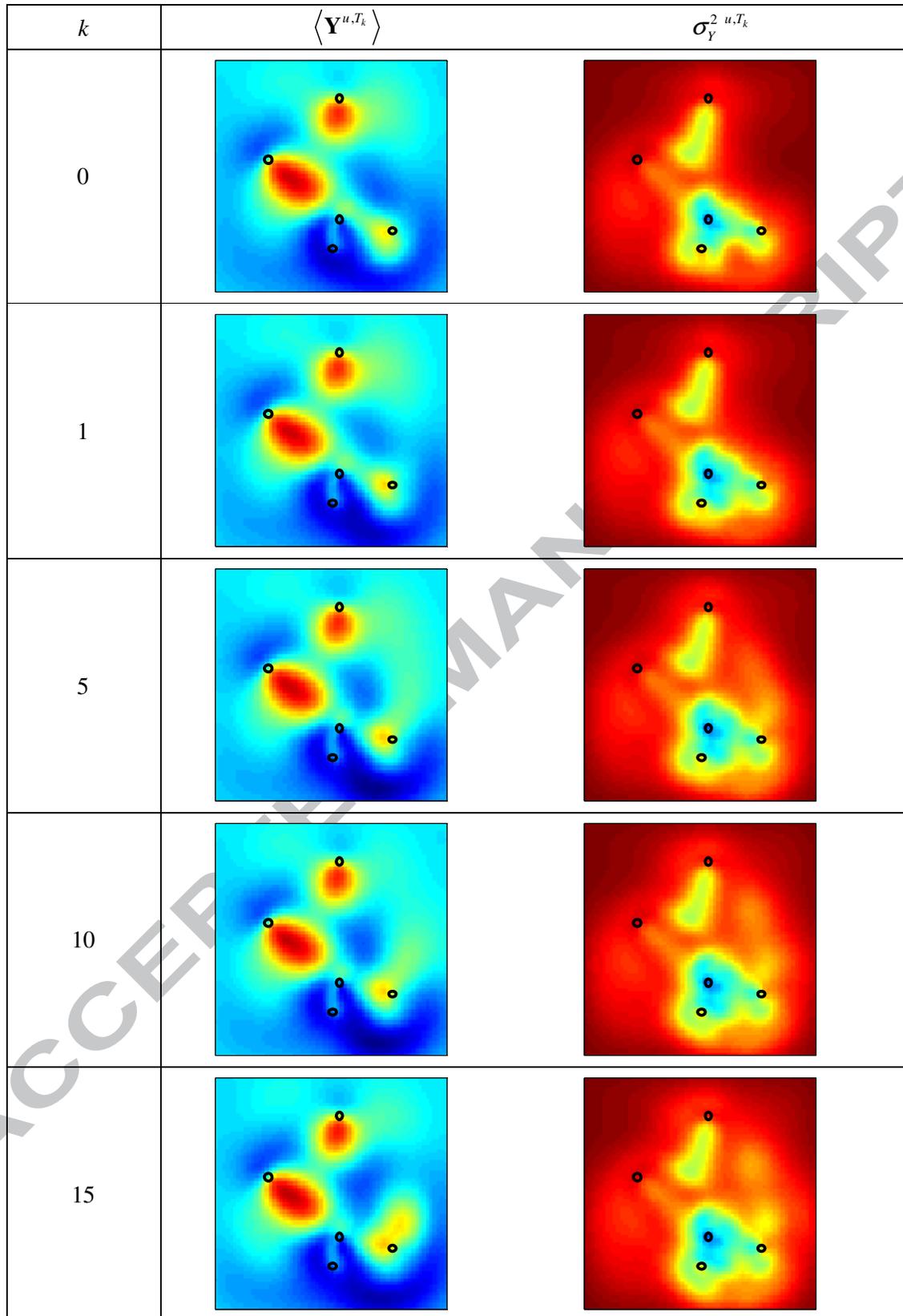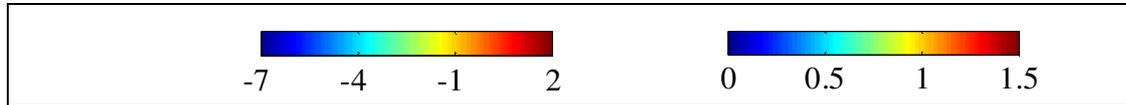
Figure 6. Spatial distributions of estimated log transmissivity mean and variance at assimilation steps *k* of drawdowns measured during test T3 while pumping well B3 and following assimilation from test T2. Circles indicate spatial locations of wells B1 - B5.
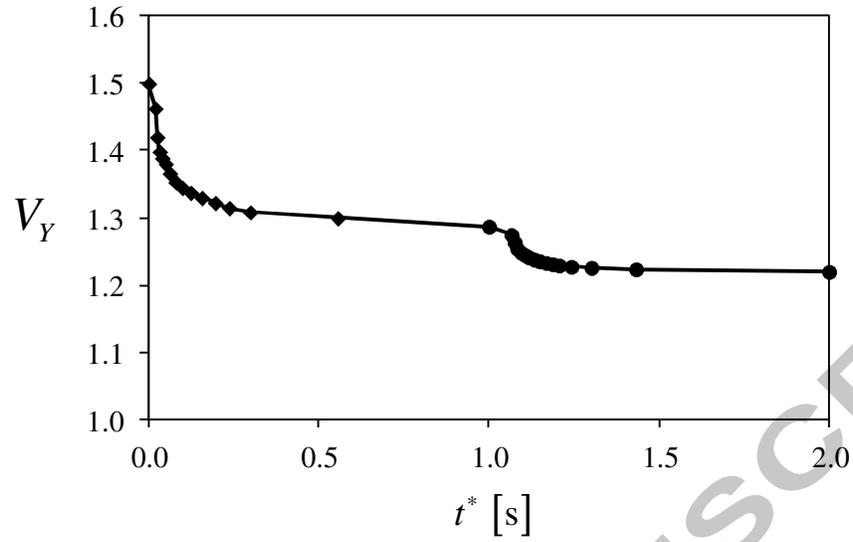
Figure 7. Spatially averaged estimation variance, V_Y (7), versus normalized time ($t^* = T_k / T_{N_k}$) during assimilation of drawdowns while pumping well B2 ($0 < t^* < 1$) and subsequently well B3 ($1.0 < t^* < 2.0$).
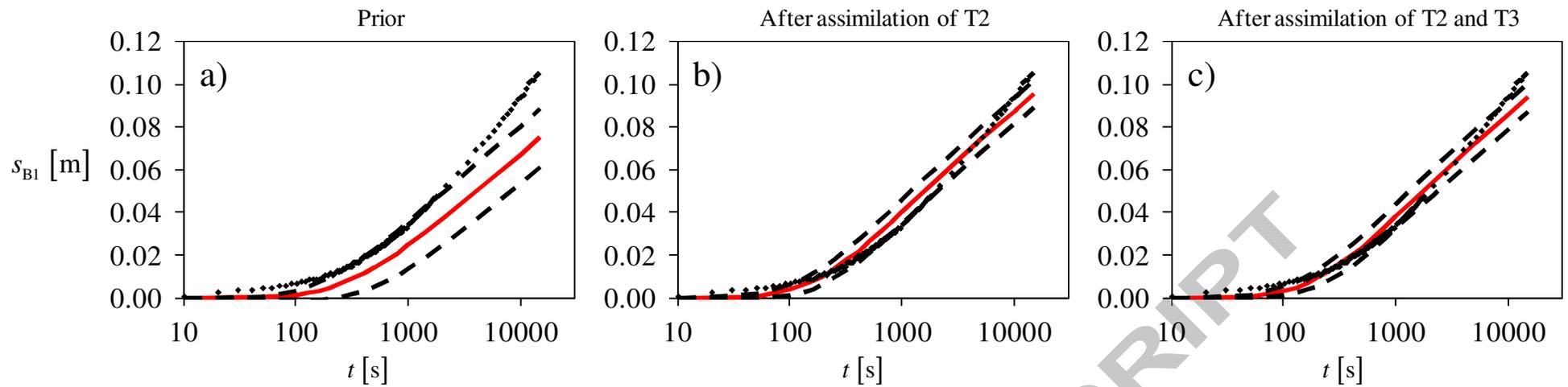
Figure 8. Drawdown measured at well B1 while pumping well B4 (symbols) in test T4, estimated mean (red curve) with ± two standard deviations confidence intervals (dashed curves) obtained with log transmissivities (a) prior to data assimilation, (b) after assimilation of T2 data, and (c) after joint assimilation of T2 and T3 data.
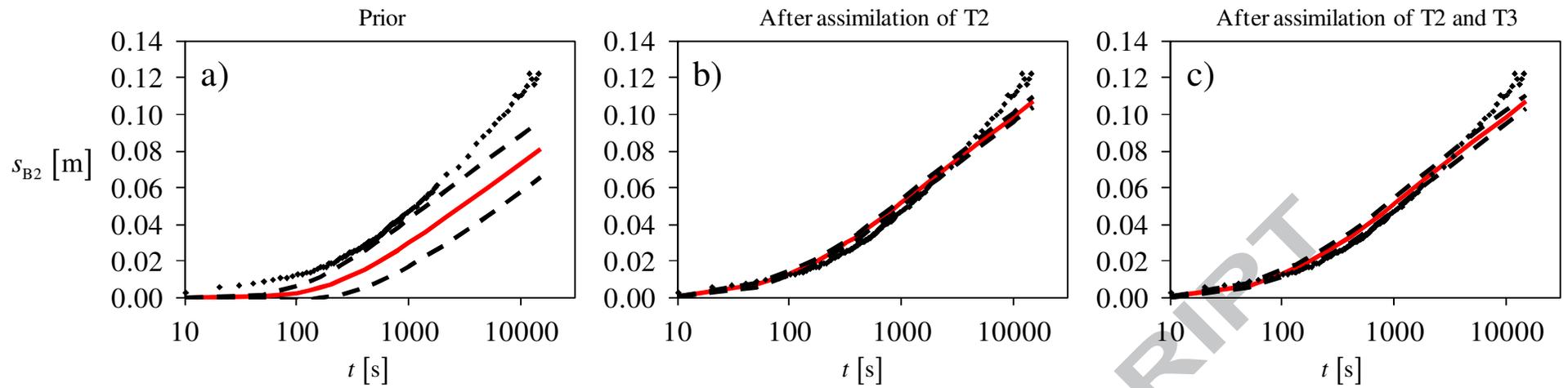
Figure 9. Drawdown measured at well B2 while pumping well B4 (symbols) in test T4, estimated mean (red curve) with ± two standard deviations confidence intervals (dashed curves) obtained with log transmissivities (a) prior to data assimilation, (b) after assimilation of T2 data, and (c) after joint assimilation of T2 and T3 data.
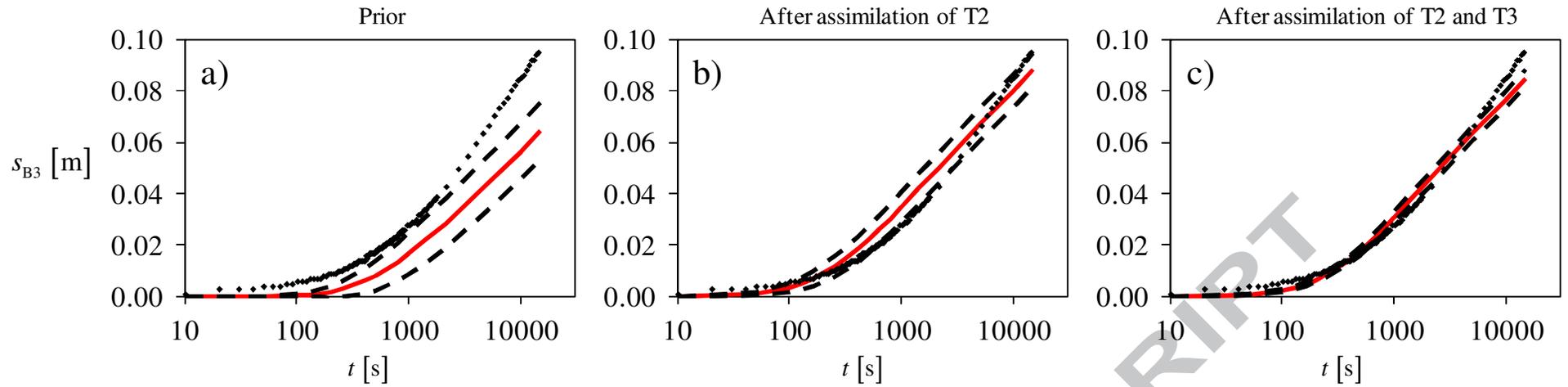
Figure 10. Drawdown measured at well B3 while pumping well B4 (symbols) in test T4, estimated mean (red curve) with ± two standard deviations confidence intervals (dashed curves) obtained with log transmissivities (a) prior to data assimilation, (b) after assimilation of T2 data, and (c) after joint assimilation of T2 and T3 data.
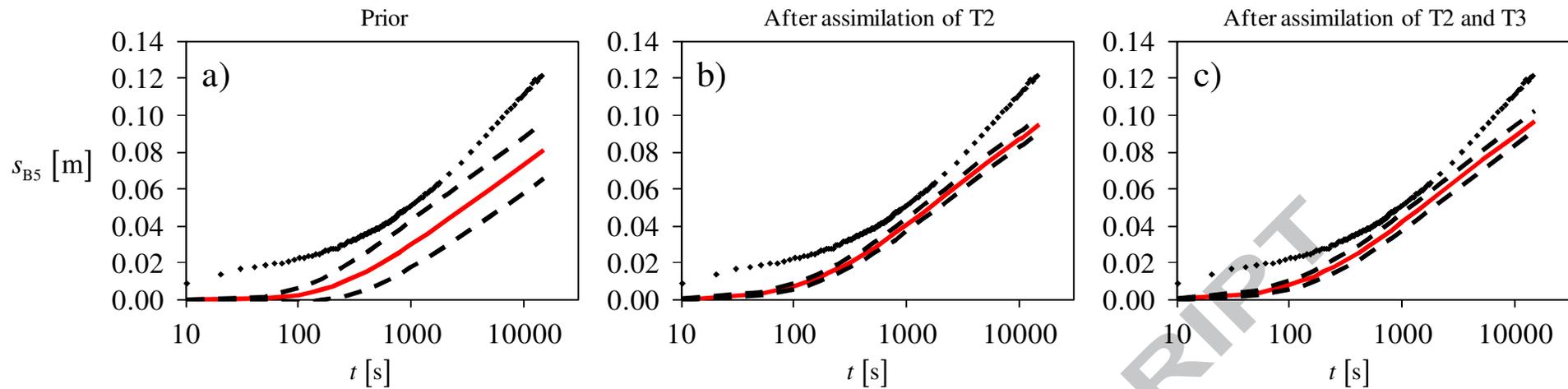
Figure 11. Drawdown measured at well B5 while pumping well B4 (symbols) in test T4, estimated mean (red curve) with ± two standard deviations confidence intervals (dashed curves) obtained with log transmissivities (a) prior to data assimilation, (b) after assimilation of T2 data, and (c) after joint assimilation of T2 and T3 data.
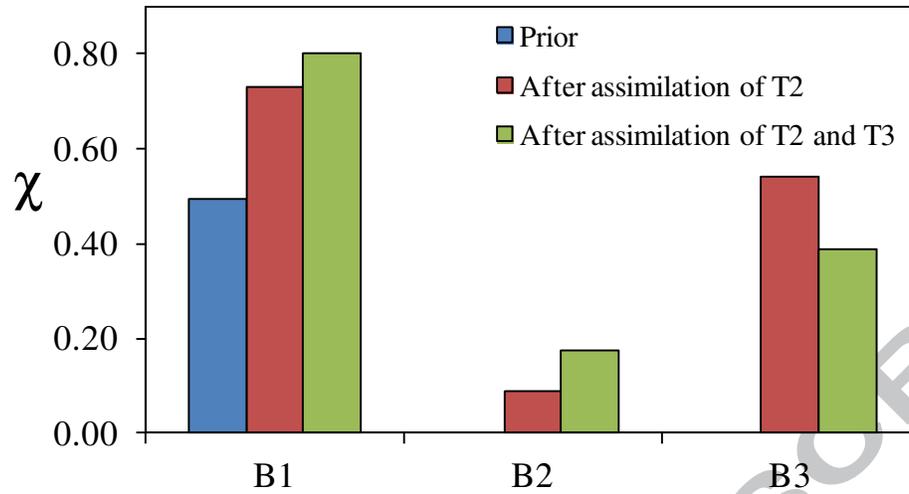
Figure 12. Percentage χ of drawdowns during pumping test T4 within uncertainty bounds of ± 2 standard deviation about mean based on prior *Y* estimates (blue), estimates obtained after assimilating T2 data (red) and after subsequent assimilation of T3 data (green).

k	$\left\langle \mathbf{Y}^{u,T_k} \right\rangle$	$\sigma_Y^{2\ u,T_k}$
0		
1		
5		
10		
15		
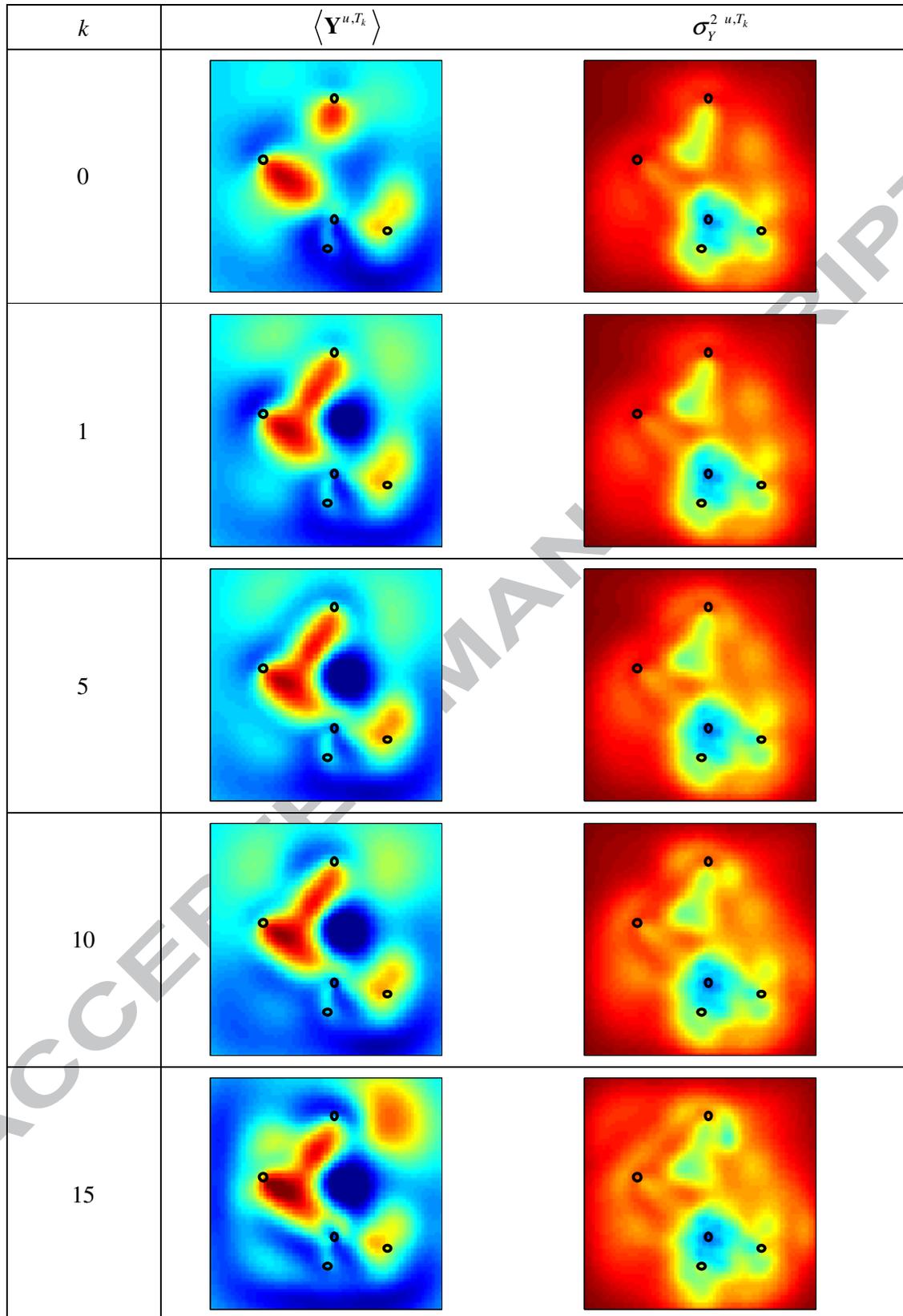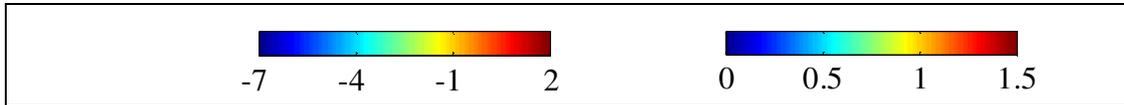
Figure 13. Spatial distributions of estimated log transmissivity mean and variance at assimilation steps *k* of drawdowns measured during test T4 while pumping well B4. Circles indicate spatial locations of wells B1 - B5.
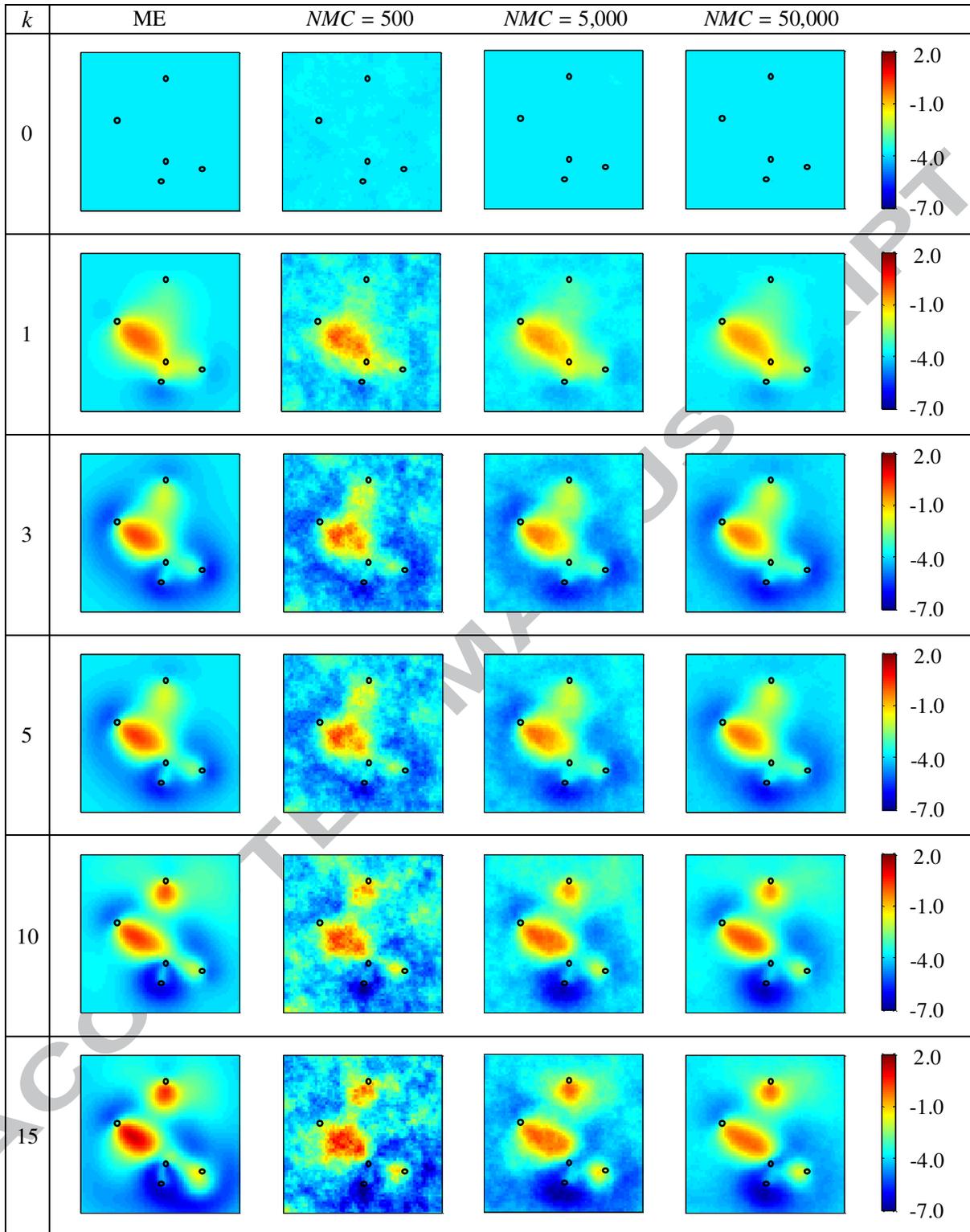
Figure A.1. Spatial distributions of estimated log transmissivity mean at assimilation steps k of drawdowns measured during test T2 while pumping well B2 using the ME- and the MC-based EnKF with diverse values of *NMC*. Circles indicate spatial locations of wells B1 - B5.
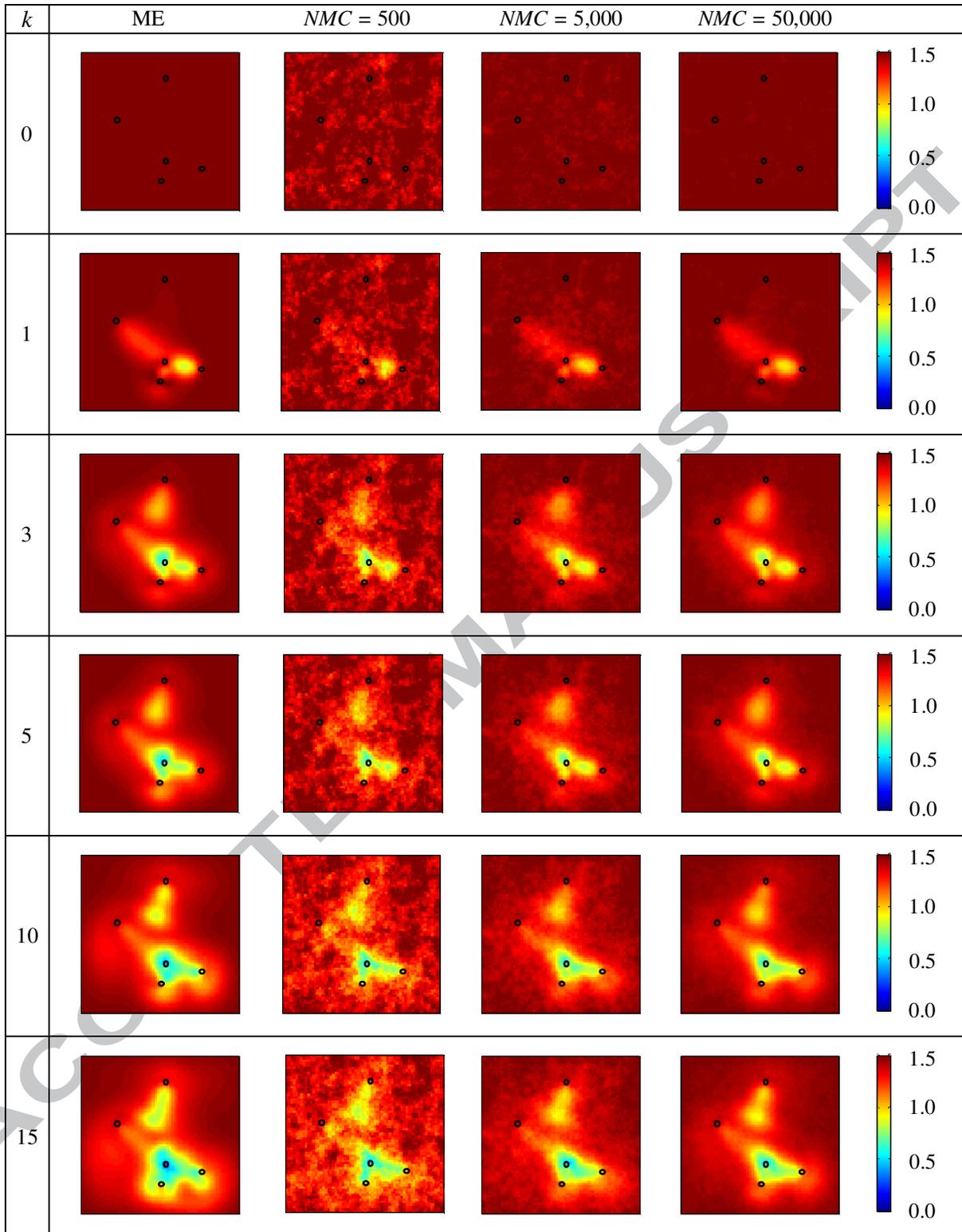
Figure A.2. Spatial distributions of estimated log transmissivity variance at assimilation steps k of drawdowns measured during test T2 while pumping well B2 using the ME- and the MC-based EnKF with diverse values of NMC. Circles indicate spatial locations of wells B1 - B5.

Test Name	Pumping Well	Pumping flow rate [m^3/s]	Duration [*hours*]	Average initial saturated thickness [m]
T2	B2	$5.27{\times}10^{-3}$	3.46	4.81
T3	B3	$3.00{\times}10^{-3}$	3.34	5.04
T4	B4	$5.48{\times}10^{-3}$	3.93	5.64

Table 1. Pumping well, rate, duration and average initial saturated thickness in tests T2, T3 and T4.

Highlights

1. Traditional EnKF assimilation requires computationally intensive MC simulations
2. Coupling EnKF with moment equations (ME) eliminates this need and inbreeding
3. Here we use ME-based EnKF to estimate aquifer transmissivities at a field site
4. ME-based results compare favorably with those of numerous MC simulations
5. As such, ME- based EnKF requires a lesser amount of computer time